JOURNAL OF GEOPHYSICAL RESEARCH, VOL. 107, NO. A8, 1175, 10.1029/2001JA000183, 2002

Correction published 28 February 2004

A detailed study of equatorial electrojet phenomenon using Ørsted satellite observations

Geeta Jadhav, Mita Rajaram, and R. Rajaram
Indian Institute of Geomagnetism, Mumbai, India

Received 21 June 2001; revised 30 November 2001; accepted 10 December 2001; published 10 August 2002.

[1] Detailed analysis of the scalar magnetic field data from Ørsted satellite for quiet days from April 1999 to March 2000 has been undertaken to study the equatorial electrojet (EEJ) phenomenon. An objective technique has been adopted for the identification of the EEJ from the satellite data and estimation of the standard parameters associated with it. EEJ strength computed using the satellite data and simultaneous ground magnetic observatory data, for the Indian and American sectors, correlate very well authenticating the method used. Estimated zonal variation in the EEJ parameters such as peak current intensity (J_0), and total current (I_+) are broadly consistent with the earlier observations. We, however, observe that the width of the EEJ varies considerably with longitude, a feature not seen in the Pogo data. The study shows that the EEJ axis (center of EEJ) closely follows the dip equator at altitude of 106 km, but there is a small departure that undergoes diurnal variation, with a minimum at noon. The globally averaged EEJ amplitude follows the expected diurnal pattern. Principal component analysis technique reveals that first four components can explain around two thirds of the electrojet variability. The first component, which contributes a little over 30% to the observed variance, could be identified with the global variation of the EEJ emanating from the day-to-day variability of the migrating tides. The second and fourth components, which account for around 15 and 10% of the variance, respectively, are driven by forcing that depends on whether the location of the EEJ in that sector is in the Northern or Southern Hemisphere. The third component provides maximum contributions wherever the geomagnetic and dip equators are sufficiently close, accounting for 12.5% of the variance. The remaining components could be associated with contribution of nonmigratory tides or other unknown mechanisms. Thus the present study suggests that besides conductivity, atmospheric tidal modes play important role in defining the zonal variability of the EEJ current system. *INDEX TERMS:* 2409 Ionosphere: Current systems (2708); 2415 Ionosphere: Equatorial ionosphere; *KEYWORDS:* equatorial electrojet, satellite magnetic measurements, principal component analysis, longitudinal variation

1. Introduction

[2] The equatorial electrojet (EEJ) represents an enhancement of the diurnal variation in the geomagnetic field near the dip equator. Extensive studies of the EEJ have been carried out for many years using ground observations [*Rastogi*, 1989]. Study of EEJ phenomenon using satellite [*Cain and Sweeney*, 1973] has a distinct advantage that it can provide true global coverage. Following *Cain and Sweeney* [1973], a number of investigations have been carried out using the Pogo data [cf. *Onwumechili*, 1997, and references therein], which have shown that the longitudinal variation of EEJ strength cannot be accounted for by the longitudinal changes in the Cowling conductivity. Identification of meridional currents associated with the EEJ became possible with Magsat vector magnetic data [*Maeda et al.*, 1982; *Langel et al.*, 1993].

0148-0227/02/2001JA000183$09.00

[3] In the present communication we have reported the results obtained from a statistical study of the scalar magnetic field data of Ørsted satellite. The EEJ can be clearly identified on almost all the passes of the Ørsted data [*Jadhav et al.*, 2002]. The local time and altitude of the satellite for the passes during the day varies very little, and it is possible to get the electrojet strength at different longitude zones on the same day. The Ørsted satellite thus constitutes a very valuable set of data for studies of the EEJ. In our earlier study [*Jadhav et al.*, 2002], we had looked into the extent of geomagnetic main field control over the EEJ. Here, we make a more quantitative estimate of the EEJ parameters and its day-to-day variability as seen in the satellite data.

[4] In section 2, Ørsted data are briefly introduced, and the preliminary treatment required for isolating the EEJ signature is laid out. In section 3, we discuss the basic model used for the EEJ analysis, method of analysis, and different EEJ parameters that are obtained in present study. In section 4, the validation of identified parameters through

comparison with ground magnetic observations is discussed. In section 5, the statistical relationship, between the derived EEJ parameters, are discussed in detail. Section 6 examines the longitudinal and local time variation of EEJ, while in section 7, we look at the problem of the variability of the EEJ from day to day. Results and discussion have been accommodated in section 8.

2. Preliminary Treatment of the Ørsted Data

[5] The polar orbiting Danish Meteorological Institute (DMI) satellite Ørsted was launched on 23 February 1999 [*Neubert et al.*, 2001]. In the present analysis we use scalar magnetic field measurements recorded by the Overhauser proton magnetometer, on board the satellite. The data have an absolute accuracy better than 0.3 nT. The orbital period is ~100 min; that leads to ~15 day and an equal number of night passes. The longitude and local time (LT) increment is $-25°$ per orbit and -0.88 min per day, respectively. Hence, for a given date, all the daytime passes have almost the same local time. In this paper, we have analyzed 12 months of scalar magnetic field data from April 1999 to March 2000 with LT varying from 13.6 to 9.5 hours. Table 1 gives the typical local times of the passes from month to month.

[6] The signature of the EEJ becomes weaker as the height of the satellite orbit increases. As disturbances of magnetospheric origin can mask the typical signature of the EEJ at the orbit of Ørsted, the analysis has been restricted to geomagnetic quiet days. Only the data from the 5 International Quiet Days (IQ) of each month is used in the analysis. This does not grant immunity against intrusions of magnetic disturbance effects considering the fact that we are close to the solar maximum and few days are entirely free of geomagnetic disturbances. The main field is removed using IGRF 2000, supplied by Ørsted team [*Olsen et al.*, 2000]. The basic inputs for the main field computation are the satellite location and the hourly *Dst* values which are readily available at the World Data Centers (WDCs).

[7] The residual magnetic field ΔF includes fields produced by external current sources like the EEJ, Sq, and magnetospheric currents. This is subjected to low pass filtering using 203-point sine-terminated low pass filter with least squares approximated transfer functions [*Behannon and Ness*, 1966] to remove spatial wavelength less than 4°, before it is used to identify the EEJ. A typical EEJ signature in the satellite profile has been clearly described by *Cain and Sweeney* [1973]. The expected latitudinal profile is shown in Figure 1. The signature is characterized by a minimum at the latitude of the EEJ axis accompanied by "shoulders" of increased field on either side. Vertical distance between dip and shoulders (CC') in Figure 1, is a measure of the strength *S* of the contribution of EEJ currents at the satellite location and the horizontal distance between two shoulders (WW') gives the width of signature at satellite height of the EEJ current system. The Pogo and Magsat satellite studies successfully used this typical signature for identifying the EEJ. It is therefore adopted in the analysis of the Ørsted data.

Table 1. Local Times of the Passes in Different Months

Month	LT, hour
1999	
April	13.6
May	13
June	12.7
July	12.5
August	12
September	11.5
October	11
November	10.5
December	10
2000	
January	9.5
February	9
March	8.5

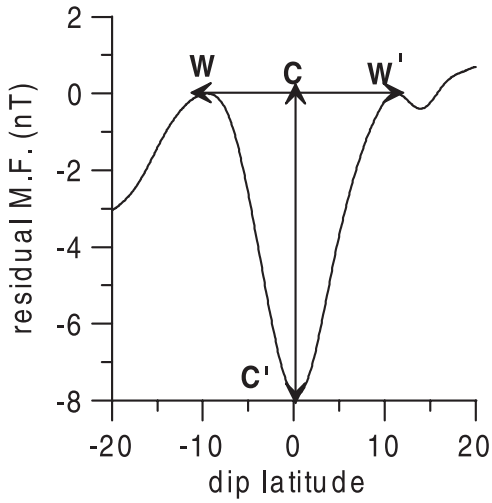

Figure 1. Typical signature of the latitudinal profile of the residual field observed at Ørsted satellite height for 135°E longitude pass, on 2 August 1999.

[8] A Fortran program was developed to automatically identify EEJ signatures from the selected satellite orbital data restricted to ±20° dip latitude and to process and store the transformed data useful for evaluation of the EEJ parameters. Out of 839 passes, only those that showed a well-defined minimum within ±5° of the dip equator were considered. The program takes care of the following alternatives:

1. The minimum is accompanied by two maximum values, one on either side; those positions of maxima define the edges of the EEJ.

2. The second maximum is only registered as a change in gradient; this is considered as the second edge.

3. Only one maximum is identified; a point symmetrically located on the other side of the minimum is taken as the position of the second edge.

4. Neither of the two maxima is discernible; in this case edges are assumed to be located at ±12°.

[9] A linear trend is removed to bring the two edges to the same level. In case of 2, 3, and 4 a cubic fit to our low-latitude data segment outside the EEJ belt (defined by two edges of EEJ) is removed. These two steps are repeated (maximum of 5 times) in attempt to get the ideal situation defined in case 1.

[10] The entire ΔF profile for each of the passes, consisting of around 300 to 350 data points, is used for obtaining the EEJ parameters. The 513 ideal EEJ signature passes as well as the 267 passes for which the signature was clear in one hemisphere and suggestive (but not so explicit) in the other hemisphere are used for the statistical study of estimates of the EEJ parameters. It should be mentioned in passing here that 45 of the satellite ΔF profiles had distinct reversed EEJ signature. Data from these passes are not used in this analysis.

3. Determination of EEJ Parameters

[11] We shall take the point of view that the typical signature at satellite altitude above EEJ current system shown in Figure 1 is associated with an eastward current flowing near dip equator and westward current on both flanks of the magnetic dip equator. We use the model for EEJ due to *Onwumechili* [1997, p. 145], which can reproduce the dip as well as the shoulders seen in the satellite. The northward, X and vertical, Z components of the magnetic field from the continuous distribution of current density model

$$J = J_0 \frac{(a^2 + \alpha.x^2)}{(a^2 + x^2)^2} \frac{b^2}{(b^2 + z^2)^2}$$

is given by [*Onwumechili*, 1997, p. 279]

$$(sg \cdot z)P^4 X = \frac{1}{2} Ka \Big[(v + \alpha v + 2\alpha a)(u + b)^2 + (v + \alpha v + 2a)(v + a)^2 \Big] \quad (1)$$

$$-(sg.x)P^4 Z = \frac{1}{2} Ka(u + b) \Big[(1 + \alpha)(u + b)^2 + (v + \alpha v + 3a - \alpha a)(v + a) \Big], \quad (2)$$

where $P^2 = (u + b)^2 + (v + a)^2$, $K = 0.2\pi J_0$,

$$u = |x|,\ v = |z|,\ sg \cdot x = \text{sign of } x = \frac{x}{u},\ sg \cdot z = \text{sign of } z = \frac{z}{v}.$$

[12] Here, the center of the current system has been taken as the origin, x is the latitudinal distance measured northward from the origin, y is eastward, and z is vertically downward distance from the current layer. The a and b values are latitudinal and vertical scale lengths, respectively, α is dimensionless constant controlling latitudinal distribution of current, J_0 is the peak current intensity or the height-integrated current density at the center of the current system. If X and Z are in nanoteslas, then J_0 is in Amperes/km.

[13] The identification of the EEJ parameters is based on the above empirical model. Many of the earlier studies [e.g., *Onwumechili*, 1997 p. 296] had used the same model, but they based their estimations on the magnitude S (defined in section 2) and did not make use of the full EEJ signature at the satellite location. In order to derive the parameters K, a, and α they assume that given the longitude and local time, these parameters do not vary from day to day. Using different sets of (S, h), where S is the EEJ strength at EEJ axis at altitude h of the satellite, they solved the above equations to get K, a, and α. However, we find that the shape of the signature (i.e., width and strength) changes from day to day even at a given longitude and LT. Hence we have computed parameters K, a, and α for each pass using 300 to 350 data points defining the structure identified and stored by the process described in section 2.

[14] For the estimation of the EEJ parameters we have assumed that the EEJ current flows at a height of 106 km in the ionosphere and neglected the subsurface induced currents for computing the field at the satellite height. There is some justification in making such assumptions. A number of rocket measurements in the equatorial region have confirmed that the peak electrojet current flows at 106-km altitude [*Sampath and Sastry*, 1979]. *Fambitakoye and Mayaud* [1976] found no measurable induction of the electrojet field in Central Africa, while *Ducruix et al.* [1977] have shown theoretically that electrojet-induced field is negligible at least along the noon meridian. *Yacob* [1977] examined internal induction by the EEJ in India with ground and Pogo satellite geomagnetic observations and found that its internal field contribution is small. This could be regarded as some justification for neglecting geomagnetic induction. Furthermore, subsurface conductivity is also a variable quantity and making even intelligent guesses of its underlying longitudinal structure would lead to a bias in the estimated induced currents.

[15] The scalar field $\Delta F \left(= \sqrt{X^2 + Z^2}\right)$ is computed using equations (1) and (2). For each EEJ pass, parameters a and α are varied iteratively until they produce shoulders at right locations. The parameter K is obtained through least squares fit to ΔF along the satellite profile that incorporates a constant background shift. The best fit is decided by the cross correlation between the observed and computed profiles as well as the mean square differences between them. The parameter set with lowest mean square difference and a cross correlation greater than 0.7 is selected. The methodology is fully automated and objective. However, it has to be tested with independent data to establish its authenticity and statistical reliability. This is achieved in section 4 through the comparison of H (the horizontal component of the magnetic field) of the observatory magnetic field data with the H variation on ground computed using overhead satellite measurements.

4. Comparison Between Satellite and Ground Observations

[16] For comparisons, we use observatory data with dip latitude λ, geographic longitude ϕ, from Trivandrum (λ = 0.43°, ϕ = 76.9°E) and Alibag (λ = 13.06°, ϕ = 72.9°E) in the Indian sector and Huancayo (λ = 0.59°, ϕ = 284.7°E) and Fuquene (λ = 17.11°, ϕ = 286.3°E) in the American sector. The comparison with ground data was made from pass to pass. Identification of the EEJ on ground requires at least two stations, one close to the dip equator (the electrojet station) and the other a low-latitude station (nonelectrojet station) just outside the influence of the EEJ [*Bhargava and Yacob*, 1973]. Comparisons were possible only when the satellite passed within longitude range of ±5° of the longitude of the stations or when there were at least two passes in

a day within longitude range of ±30° of the longitude of the chosen stations. In the first case the field on ground was calculated using the parameters determined for the given pass. In the second case the field computed at the two longitudes corresponding to the satellite passes were interpolated to obtain the field in the longitude zone of the given chosen stations. In doing so, it has been tacitly assumed that the EEJ field has the same local time (LT) pattern at neighboring longitudes and the two values around 100 min apart can still be used for interpolating in longitude to get EEJ field at the given longitude and LT. Equation (1) is used to obtain the EEJ contribution to H at any latitude.

[17] For estimating the EEJ field on ground in the Indian sector, hourly values of Trivandrum and Alibag magnetic observatories were used. Nighttime means were subtracted from the daytime hourly values, and these were interpolated to determine the H at the local time of the crossing of the Ørsted satellite. The interpolated value for Alibag was subtracted from that at Trivandrum to obtain the instantaneous value of $EEJH_{obs}$ at the time of satellite overhead crossing. Similar data reduction techniques were utilized for Fuquene, but in the case of Huancayo, the daily traces had to be down loaded from WDC, Kyoto site and redigitized.

[18] The estimate of the electrojet strength on ground from the satellite parameters is obtained by computing the H at the axis of the EEJ current system as deduced from the satellite data. The correlations between $EEJH_{obs}$ (the observed electrojet strength on ground) and $EEJH_{computed}$ (the estimated strength based on the satellite data) are presented separately for American (Figure 2) and Indian (Figure 3) sectors. The scatter is symmetrically distributed about the mean regression line, and the correlation coefficient is 0.86 in both Indian and American sectors. This compares favorably with the results of *Yacob* [1977], who found correlation coefficient of around 0.88 between the surface electrojet strength observed in the Indian region, extrapolated to the satellite height using a parabolic current-band model of electrojet, and the strength as obtained from satellite measurements. These correlations for the given number of points are significant at 99.9% level. The excellent match confirms that the algorithm used has provided reliable estimates of a and K and fully authenticate the technique used for deducing the EEJ parameters from the satellite data. Subsurface currents are expected to add to the surface H, and the slope of regression line is probably greater than unity because of the neglect of the induction effect. We do not claim a perfect estimation from pass to pass, but it can be justifiably argued that the estimations should provide the basis for the investigations of the statistical properties of the EEJ in different longitude regions around the globe.

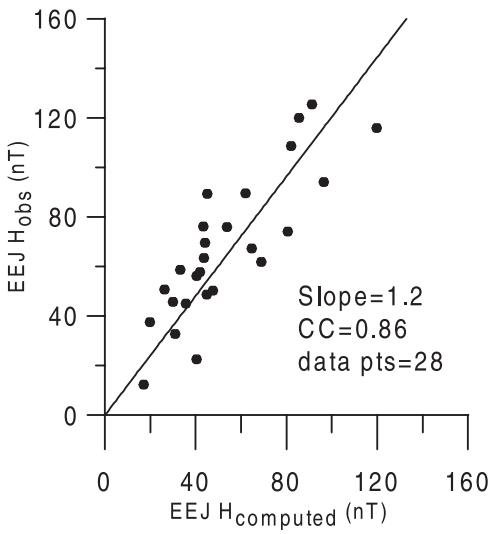

Figure 2. Scatterplot of equatorial electrojet (EEJ) H_{obs} from American observatory data plotted against the EEJ $H_{computed}$ computed at the axis of EEJ from satellite based EEJ parameters.

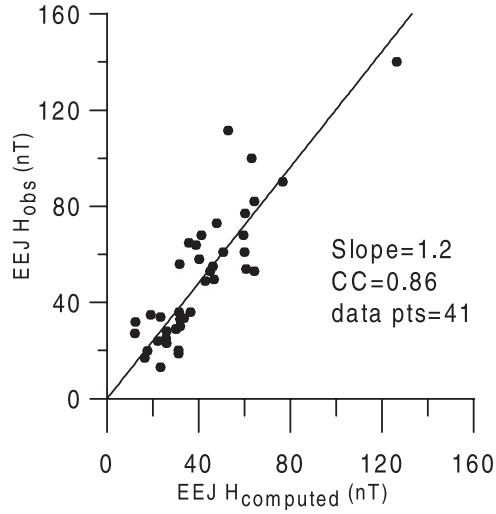

Figure 3. Same as Figure 2, for Indian region.

5. Statistical Relationship Between EEJ Parameters

[19] There are four main parameters of the EEJ whose longitudinal variations have been discussed in literature [*Onwumechili*, 1997]. These are the peak of the EEJ current given by J_o, the position of the electrojet axis x_o, the estimated width of the EEJ given by $W = 2a/\sqrt{-\alpha}$ and I_+, the total amount of positive eastward current in amperes flowing between the two locations of zero intensity given by

$$I_+ = aJ_o\left[(-\alpha)^{1/2} + (1+\alpha)\tan^{-1}\left(\frac{1}{-\alpha}\right)^{1/2}\right]. \qquad (3)$$

[20] In discussion, we also mention the width of EEJ at satellite and ground. The width of EEJ at satellite ($W_{satellite}$) is the direct observation of the distance between two peaks in the EEJ signature at satellite altitude and that on ground (W_{ground}) is the distance between two minima in the EEJ signature computed on ground from the model parameters. The overall nature of the parameters derived from the satellite data is depicted in Figures 4a–4e. There is a clear positive correlation between J_o, the peak current density and H_{axis}, the computed field at the EEJ axis on ground (Figure 4a). The scatter about the fitted straight line may

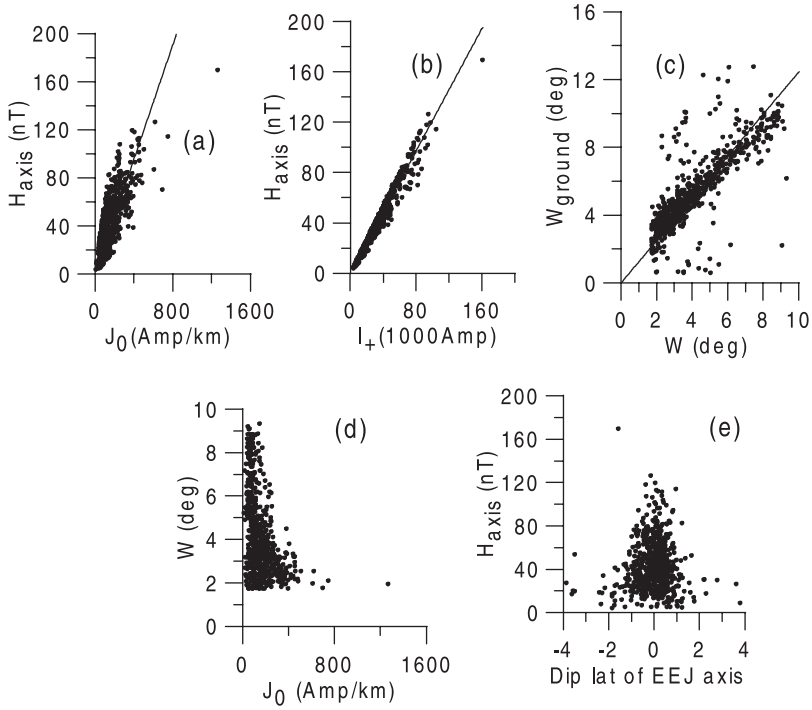

Figure 4. Scatterplot for EEJ parameters determined from satellite data. See text for definition of parameters.

be mainly attributed to variability in a. This scatter is not an indication of errors but only emphasizes the fact that the surface field is not entirely determined by the peak current density. This is brought out by the reduced scatter in the straight-line fit when I_+ is used instead of J_o (Figure 4b). This reduction in scatter shows that I_+ and not J_o is more relevant as far as ground magnetic effects are concerned.

[21] The relationship between W_{ground}, and the width W at the position of current system (Figure 4c) is linear, but there is also a scatter that underlines the fact that two independent parameters a and α together determine the relationship between the width of EEJ at ground and 106 km, which is therefore not simple and straightforward. The relationship between $W_{\text{satellite}}$ and W_{ground} that is not plotted here is also linear, but the width at the satellite height is $\sim$3 times the width on ground.

[22] Relationship between J_o and the width of the EEJ (W) at 106 km is plotted in Figure 4d, which suggests that larger values of the peak current density are associated with smaller scatter in the width of the latitudinal structure of the electrojet. This scatter may probably imply that when J_o is small the signature of the EEJ at the satellite heights are smaller, and hence there is a greater chance of errors creeping in derivation of the structural parameters a and α, which ultimately determine the width of the EEJ. The spread could also arise owing to the fact that smaller peak currents may require larger width to reproduce a given signature at the satellite height. The standard deviations of the spread of the width scatter are reasonable, and the parameter can thus supply reliable statistical data on the EEJ. Finally, Figure 4e shows how the position of axis of the electrojet current system (with respect to the dip equator) controls the electrojet strength on ground. The diagram clearly demonstrates the fact that strength of EEJ is considerably reduced when its axis shifts away from the dip equator. The results can be expected on physical grounds.

[23] In conclusion, Figures 4a–4e suggest that the parameters determined from the Ørsted passes are suitable for the study of the statistical properties of the EEJ, though it may not be the right choice for detailed analysis of individual case studies. In what follows, we concentrate on the statistically averaged values of the derived EEJ parameters and examine their dependence on the longitude, season, and local time. In the process we shall determine whether these are consistent with the earlier studies based on Pogo and Magsat.

6. Longitudinal and Local Time Variation of EEJ

[24] In this section, we examine the longitudinal and local time structure of the EEJ parameters derived from satellite observations. In Figure 5, we plot the longitudinal variation of average values of the current parameters I_+, J_o, and W in the ionosphere, while in Figure 6 we look at the magnetic field on the ground at the axis of the current system. Each point, in these figures represents an average of all the passes in a 30° bin centered at longitudes 5°, 15°, 25°, etc. In these plots, as well in all the plots that follow, the error bar corresponds to the estimated standard error of the mean.

[25] The peaks in the total eastward current I_+ (Figure 5a) are in broad agreement with those determined for the Pogo satellite data by *Onwumechili and Agu* [1981]. Note also that the longitudinal variation of the EEJ strength on ground (Figure 6, left topmost) is almost identical to that of I_+ but not to J_0. *Onwumechili and Agu* [1981] get three well-defined

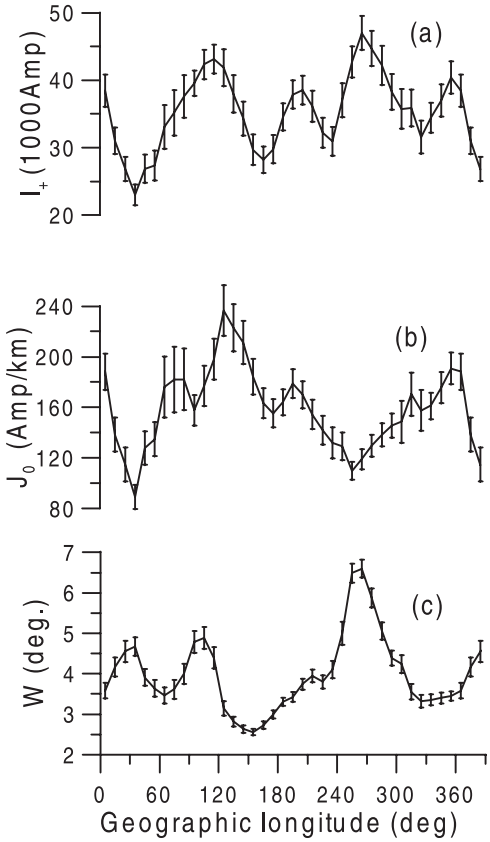

Figure 5. Longitudinal structure of (a) I_+, (b) J_0, and (c) the electrojet width W plotted as a function of longitude. Error bars are estimated variance of the mean.

peaks for J_0 centered at 100°, 190°, and 270°E and a smaller peak around 350°E. We do not get the peak at 270°E. Furthermore, the magnitudes of the peaks are less in our case, and two less clearly defined peaks at 70° and 120° replace the peak at 100° obtained by them. The dusk time horizontal currents deduced from Magsat analysis [*Langel et al.*, 1993] revealed peaks at 280°E and between 110° and 150°E but showed no clear peak around 100°E. However, some of their figures depicting eastward electrojet signatures do show indications of peak at 360°E and around 180°E.

[26] Figure 5c shows that the width of the EEJ current system is largest in the American sector, and this is responsible for the strong peak in the EEJ strength at 270°E, though it is not reflected in J_0. Larger width of the current system will be associated with larger a, and it is not difficult to see from equations (1) and (2) that this will lead to larger magnetic field on ground. There are also two secondary peaks at 30° and 105°E longitudes. The peaks are well defined and statistically significant. The width varies from 2.5° in the region 150°E to as much as 6.5° in the American zone. Though the width of 4° obtained for the Indian zone is fairly consistent with the halfwidth of 2.9° reported by *Oko et al.* [1996] using observatory data, the variation of the width of EEJ current system with longitude is much greater than that reported by *Onwumechili and Agu* [1981].

[27] A simple theoretical explanation based on increased ionospheric conductivity [*Cain and Sweeney*, 1973] cannot explain this multipeak structure (Figure 6, left topmost), and this may have to be attributed to tidal variability. It should be noted that we are discussing longitudinal structures averaged over a range of seasons/LT, and thus many of the seasonal and LT influences remain hidden. Some of these are reflected in the remaining plots of Figure 6. Plots on the left-hand side show average amplitude of electrojet strength on ground for different months labeled as March (February–March 2000, 0820–0910 LT), June (May–July 1999, 1210–1320 LT), September (August–October 1999, 1040–1200 LT) and December (November 1999 to January 2000, 0920 to 1040 LT). The right-hand side plots show amplitude averages for different local times labeled as 0830 to 0930 (17 January to 27 March 2000), 0930 to 1030 (30 November 1999 to 9 January 2000), 1030 to 1130 (8 September to 15 November 1999), 1130 to 1230 (4 July to 6 September 1999) and 1230 to 1330 (25 April to 30 June 1999).

[28] The peak around 0°E is persistent right through while the peak around 270°E remains from June to September. The peak around 110°E is most clearly seen from March to June. At 1100 LT, peak at 110° splits into two; one appears at 90° and the other at 125°. Around 180°–200°E, where the geographic and geomagnetic equators are coincident, the peak is very distinct only from December to March. The LT plot shows that the peaks in this sector are largest between 0830 and 0930 LT, where it is comparable with that of the other peaks at 1100 LT. As LT increases, its strength decreases while the peaks at other longitudes start building up. We examined the data at Jarvis Island (λ = 1.11°; ϕ = 199.97°E) and did not find any unusual LT traits that could justify such an early LT peak in EEJ. This

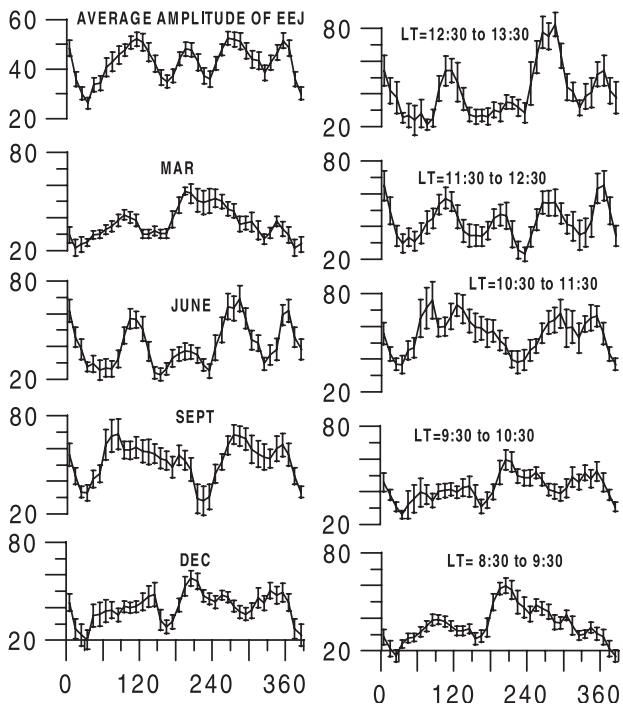

Figure 6. The longitudinal variation of the computed strength of the EEJ (nanoteslas) on ground at the position of the axis. The top plot shows the average pattern, the bottom left depicts the variations categorized in to different months, while the bottom right shows the variation categorized in terms of the local time of the satellite pass.

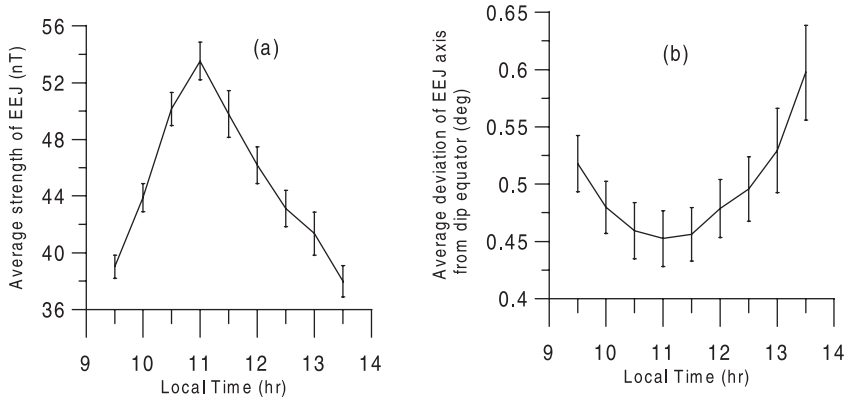

Figure 7. (a) The mean electrojet strength H on ground and (b) the shift of the latitude of the axis of the EEJ from the dip equator are plotted as a function of local time.

suggests that we are looking at a seasonal effect, and this particular peak would probably have been much larger if the satellite pass had been around noon in December to March sector. Similarly, the fact that the field at 270°E is found to be largest between 1230 and 1330 LT may also be attributed to a seasonal effect. Baring a couple of these sectors, elsewhere the peaks at 1030 to 1130 LT dominate indicating that the LT dependence that is probably most apparent. This can be seen in the mean picture presented next.

[29] We have already noted from Figure 4e that the EEJ strength on ground decreases as its axis moves substantially away from the dip equator. This is further substantiated by the results presented in Figures 7a and 7b. In Figure 7a we have shown the variation of the mean field on ground at the axis of EEJ current system, as a function of the local time of the pass. While in Figure 7b we depict the mean of the magnitude of the deviation of the position of the axis of the EEJ current system with respect to the dip equator. The mean is taken over data from all the longitude zones. The electrojet strength on ground shows the expected temporal variation peaking around 1130 LT and decreasing on either side. The position of the EEJ current axis also shows a systematic temporal pattern being closest to the dip equator around the time when the H on ground maximizes. This is consistent with the scatterplot depicted in Figure 4e, but more importantly, it corroborates the findings of *Fambitakoye and Mayaud* [1976], who also found that the EEJ current axis is located closest to the dip equator near local noon. This definitely adds credibility to the algorithms used here.

[30] We next look (Figure 8a) at the magnitude of the shift of the axis of EEJ current system from the dip equator as a function of longitude averaging over all LT (or months). Note that with the exception of regions close to 150°E, the EEJ current axis shifts away from the dip equator toward the geographic equator. These results are consistent with those of *Cain and Sweeney* [1973]. This feature is fairly persistent whether data is classified by month (Figure 8b) or by LT (Figure 8c). In the longitude regions near 30°E, 285°E and 315°E, the deviation of EEJ axis from the dip equator is systematically larger (>0.5°). The plots appear less systematic when classified according to season than according to LT. This adds credence to the argument, that the movement of the position of center of EEJ system depicted in Figure 8c, represent genuine LT variations adding strength to the conclusions arrived at in the last section.

7. Day-to-Day Variability in Surface Magnetic Field

[31] What we have examined so far is the average pattern. Of much greater relevance is the variability from day to day. There is a longitudinal dependence of the EEJ strength because the Cowling conductivity that is responsible for the electrojet has a longitudinal dependence [*Cain and Sweeney*, 1973; *Jadhav et al.*, 2002]. The next question that one asks is whether the EEJ strength strictly follows the longitudinal structure defined by the conductivity every day. We have already seen from the average picture that the longitudinal structure of the EEJ is not determined entirely by conductivity. Since tides may be responsible for at least some of the peaks, we suspect that the day-to-day variability will have a clear longitudinal structure. A recent paper by *Chandra et al.* [2000] clearly shows that the longitudinal variation of EEJ is not due to the variation of the conductivity, but due to local electric field in the ionosphere.

[32] *James et al.* [1996] studied the day-to-day variability using latitudinal array of stations in a narrow range of longitude and found that the correlation of ΔH at any station with equatorial station decreases as latitude of the station increases. *Rangarajan* [1992] using method of linear predictor filters have examined the relation between EEJ variations, at two ground stations separated in longitude. He was able to demonstrate that the electrojet H at Addis Ababa could be predicted fairly efficiently, given the time series of Trivandrum. The method is not easily applicable with satellite database of the type we have. *Schlapp* [1968] studied the variability of the EEJ from one day to another using coefficient of cross correlations between ground geomagnetic stations. He found that correlation drops to less than 0.5, if two stations are separated by 40° in longitude. We propose to use a similar cross-correlation technique with the satellite data. The satellite data cover areas of the globe not accessible to surface measurements and can be expected to provide a more complete information. Right through this section EEJ strength represents the magnitude of the electrojet on ground calculated using parameters derived from satellite observations.

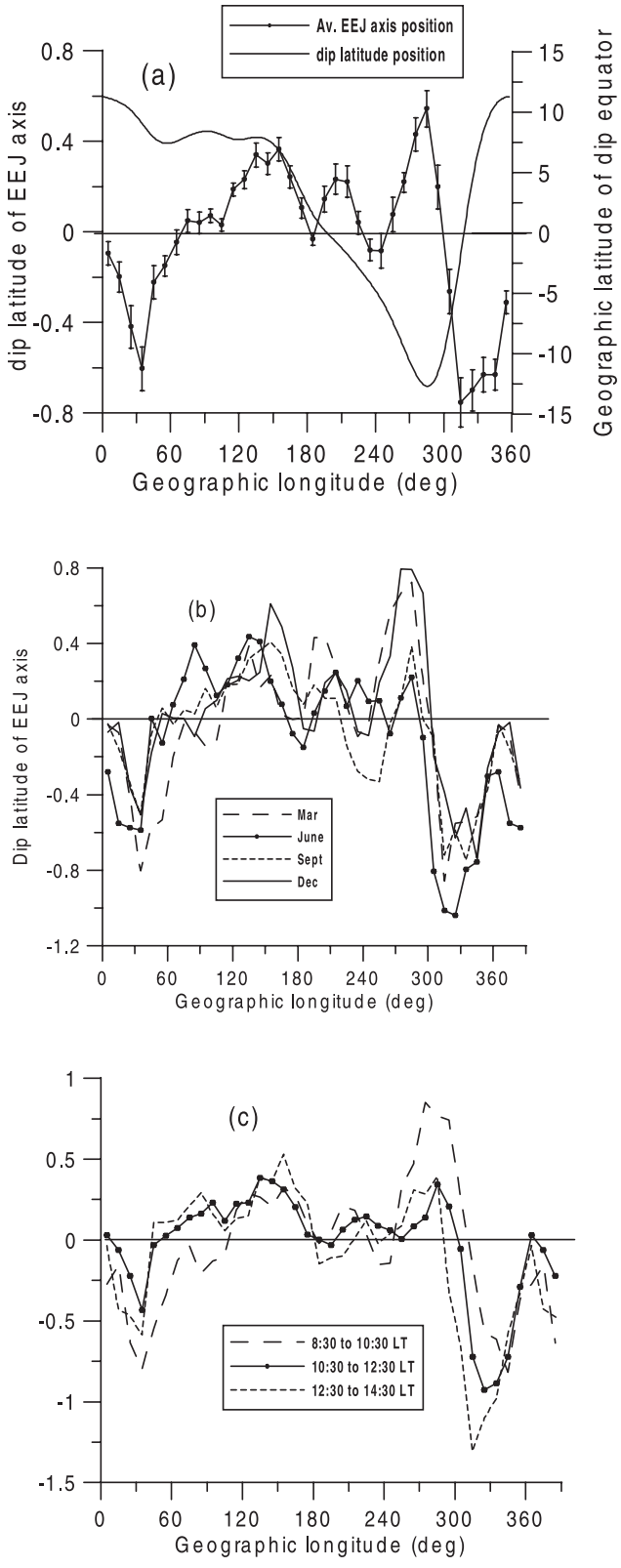

Figure 8. The mean position of the electrojet axis with respect to the dip equator is plotted as a function of longitude with the corresponding variation of the latitude of the dip equator in Figure 8a. The position of the electrojet axis with respect to the dip equator is also plotted for different months (Figure 8b) and different local times (Figure 8c).

[33] The satellite can provide 14 to 15 crossings of the dip equator per day and may be expected to provide an excellent database for the correlation analysis. In practice, however, a number of longitude sectors are missed out each day. This is not a very serious problem because the total number of useful passes is still adequate. The longitude sectors have to be divided into a number of zones for the type of analysis undertaken. We use 20° bins, and 18 of them cover the entire globe. The next problem arises because the pass need not pass through the center of the bin, and passes that are close to the edges may not be representative of the bin. There may be sometimes two passes in a day in the same bin, and sometimes the two passes in two neighboring bins may be closer to each other than to the centers they are supposed to represent. To minimize such distortions, we divide the globe into 18 equal bins in four ways, starting with the first bin centered at 0°, 5°, 10°, and 15° respectively. If ϕ_c represents the longitude of the center of any bin, then ϕ_c modulo 20 will be 0°, 5°, 10°, and 15°, respectively. The mean of these will represent bins centered at 7.5°, 27.5°, 47.5°, and so on. If there are more than two passes on any day in any of the bin, their average EEJ strength will be taken as the value at the center of the bin.

[34] Cross correlation between any two bins is calculated from all the days, which had EEJ estimates in both the bins, irrespective of availability of data in any other bin. The number of points defining the correlation between any pair varies from pair to pair but is roughly around 30 or so. The same day's data cannot be used for all pairs for obvious reasons, but this is not important as long as the number of points used for each pair is large enough for the sample to be considered representative of the population. We then take average of the four different estimates of the cross-correlation coefficients to enhance the reliability of the final estimate. The results of the analysis are presented in the correlation matrix presented in Figure 9. All values are expressed in units of 0.01, and values significant at 99% are shown in bold. The diagonal elements, which should be one by definition, are replaced, in the figure, by the variance for each bin.

[35] The variance maximizes in the Indian and American sectors. There seems no obvious explanation for this. Also note that the correlation between the EEJ in the Indian and American sectors is significant. The correlation between the American and Indian zones was simultaneously computed using the ground data of Trivandrum and Alibag in the Indian sector and Huancayo and Fuquene in the American sector. The correlation of 0.53 from the satellite observations compares well with 0.45 obtained from ground data for the same days. The correlation patterns on the whole are not systematic with even the neighboring zones exhibiting poor correlation. This may be due to rather complex forcing associated with the EEJ. We examine the correlation matrix in greater detail using powerful multivariate analysis technique.

[36] The correlation matrix is a very important entity in the multivariate analysis technique. If the EEJ at different longitudes vary independently, the matrix will have 1 as the diagonal elements and 0 for all the nondiagonal ones. If the EEJ at different longitudes vary perfectly in unison, all the elements will be one. In the real world we expect a number of patterns of forcing that may work sometimes in unison and in opposition at other times, generating a

Zone number

1	2	3	4	5	6	7	8	9	10	11	12	13	14	15	16	17	18
416	23	20	27	20	**42**	39	19	19	-16	-8	0	14	19	38	12	37	38
23	389	**55**	43	22	16	**44**	28	28	20	-5	-1	1	0	6	12	15	29
20	**55**	483	**45**	26	19	**44**	**55**	33	41	0	4	10	8	15	52	17	16
27	43	**45**	540	36	36	**48**	**52**	43	28	7	22	35	34	**53**	**63**	29	9
20	22	26	36	450	**45**	25	32	27	14	-5	-16	0	13	1	5	16	18
42	16	19	36	**45**	475	18	19	29	-13	-11	9	14	27	6	7	15	19
39	**44**	**44**	**48**	25	18	490	38	28	28	10	33	18	9	31	**57**	**50**	40
19	28	**55**	**52**	32	19	38	445	**53**	36	15	16	19	29	18	**47**	34	30
19	28	33	43	27	29	28	**53**	419	10	-5	0	-7	11	21	8	1	18
-16	20	41	28	14	-13	28	36	10	432	27	17	-3	-22	1	37	2	-17
-8	-5	0	7	-5	-11	10	15	-5	27	451	21	18	-2	9	16	5	-18
0	-1	4	22	-16	9	33	16	0	17	21	450	17	16	25	**54**	29	-26
14	1	10	35	0	14	18	19	-7	-3	18	17	414	**68**	**56**	53	40	34
19	0	8	34	13	27	9	29	11	-22	-2	16	**68**	502	**61**	**50**	35	36
38	6	15	**53**	1	6	31	18	21	1	9	25	**56**	**61**	479	49	27	23
12	12	**52**	**63**	5	7	**57**	**47**	8	37	16	**54**	53	**50**	49	466	38	23
37	15	17	29	16	15	**50**	34	1	2	5	29	40	35	27	38	454	**50**
38	29	16	9	18	19	40	30	18	-17	-18	-26	34	36	23	23	**50**	487

Figure 9. Correlation matrix in units of 0.01 by zone number. Diagonal elements are the sample variance, and the correlations significant at 99% are shown in bold face.

complex correlation matrix of the type given in Figure 9. We use the principal component analysis [*Gnanadesikan*, 1977] to determine the natural patterns of longitudinal variations of the EEJ.

[37] The basic idea of the principal component analysis is to describe the dispersion of an n component array by introducing a new set of coordinates so that the variance of the given points with respect to the derived coordinates are in decreasing order of magnitudes. In effect, instead of representing the data as values at 18 longitude points, we express it as coefficients of 18 orthogonal functions derived from the statistical property of the data itself. The variability of EEJ from day to day is represented by the corresponding variation of the coefficients of these functions. The major advantage of the technique is that the prescription of the choice of the function is such that the first few functions generally reproduce most of the variability in the data [*Rajaram and Rajaram*, 1983].

[38] Let $H_{i,j}$ be the EEJ value at the longitude ϕ_j (j = 1,18) on day d_i (i =1, N). We express $H_{i,j}$ in the form $H_{i,j} = \sum_{k=1}^{18} D_k(d_i).\Phi_k(\phi_j)$, where functions Φ_k and D_k satisfy the following constraints:

$$\sum_{j=1}^{18} \Phi_l(\phi_j).\Phi_k(\phi_j) = \delta_{lk} \quad \sum_{i=1}^{N} D_n(d_i).D_k(d_i) = \lambda_k \delta_{nk}.$$

[39] The functions Φ and D are obtained by making a least squares fit to the data itself. It turns out that functions Φ are the eigenvector of the matrix R_{jk} defined by $R_{jk} = \sum_{i=1}^{N} H_{i,j}.H_{i,k}$ and $D_k(d_i) = \sum_{j=1}^{18} H_{i,j}.\Phi_k(\phi_j)$. It is quite obvious that $\Phi_k(\phi_j)$ gives the longitudinal structure of the kth component, and $D_k(d_i)$ gives the contribution of that particular component on day d_i. The procedure is to first obtain the matrix R_{ik} from the data and determine its eigenvalues and eigenfunctions. The eigenvalues and the eigenvectors are arranged in the descending order. The percentage of the variance accounted for by the component with eigenvalue λ_k is given by $P = (\lambda_k / \sum_{j=1}^{18} \lambda_j) \times 100$. Thus the first component explains largest percentage of the variance, the second the next and so on.

[40] We express $H_{i,j}$ as departures from the mean. We further normalize it with respect to the variance of the EEJ corresponding to that longitude bin. The matrix $R_{i,j}$ then becomes the correlation matrix. There are distinct advantages in adopting this scheme. We have already noted that EEJ strength is not obtained for all longitude bins on any given day. The EEJ forcing is known to be different on different days, and it may be misleading to discuss the longitudinal structure of the variability from day to day by combining all the data together ignoring this factor. On the other hand, the correlation between any two bins is a statistic, which is reliably determined, provided the number of common days for the two bins is large enough for the sample value to be treated as the population value. Thus it is not necessary to restrict the analysis to days in which data are available in all the bins selected. Consequently, bin sizes can be taken smaller to provide better resolution in longitude. A second advantage stems from the fact that the use of correlation rather than the covariance matrix is more appropriate for identification of coherent structures [*von Storch*, 1999].

[41] We use the correlation matrices determined earlier for the four sets of bin distributions, which are generated with slight offset with respect to each other. The eigenvalues and eigenvectors are determined and ordered in descending values of their eigenvalues for each of the matrices. Each

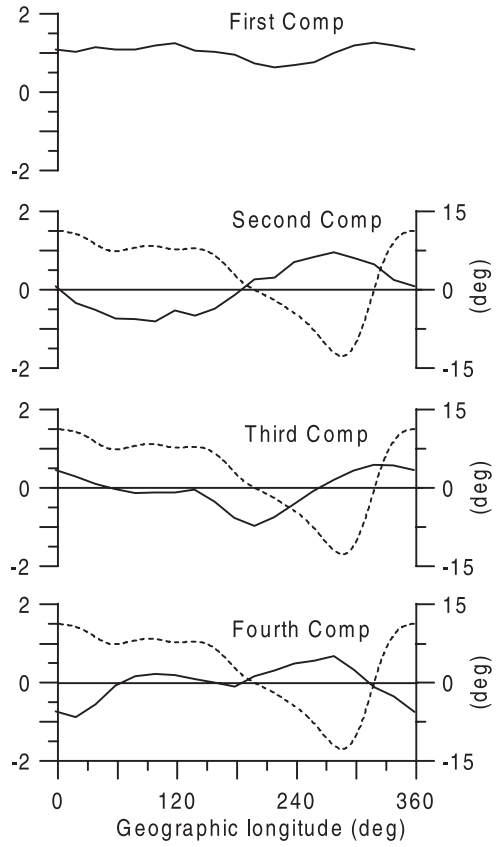

Figure 10. The longitudinal structure of the first four components obtained from the principal component analysis of the satellite data is presented. Except in first component, the profile of the latitude of the dip equator (dotted line) is also shown; the scale is shown on right-hand side.

normalized eigenvector has 18 elements, each of which represents the contribution made at the corresponding longitude bin. The 18th and the first bins are obviously contiguous. We smoothen out these contributions by taking a five-bin running mean and comparing the four different estimates we have for the longitudinal structure of the contributions corresponding to each of the four sets. We find that the first component is almost same for all the four groups. The same is true for the other components except that the structure for the bins centered at 5° (modulo 20) is slightly different. The other three are very close to each other, and the mean of 4 is also very close to them. This shows that the technique is fairly robust. Note that the overall sign of the eigenvector is irrelevant. The contribution of component is positive or negative depending upon the sign of D_k.

[42] We depict in Figure 10 the mean longitudinal structure of the first four components after multiplying contribution to each bin with the variance corresponding to that bin. This multiplication with the sample variance is necessary to make the comparison between the different longitude zones meaningful. The percentage of the variance accounted for each of the components is shown in Figure 11. The results are quite dramatic and provide considerable insight into the different types of forcing that contributes to the variability in the EEJ.

[43] The first component, which accounts for nearly 30% of the day-to-day variability, is obviously global in character except that its contribution is slightly reduced around 240°E meridian. It may be readily interpreted as the EEJ variability due to global changes in solar ionizing radiation or migratory solar and lunar diurnal, semidiurnal, and higher-order tides. The variability associated with other components appears to be generated by the longitudinal variations in separation between dip and geographic equators. The geographic equator orders the tidal forcing, while the dip equator dictates the symmetry of the conductivity of the ionosphere. To interpret these components, we have plotted the latitude of the dip equator along with each of the components.

[44] We can see that the second component, which accounts for roughly 15% of the EEJ variability, follows the latitude of the dip equator as function of longitude except a zone between 315°E and 60°E. It is exactly in this region that the component four, which accounts for 10% of the variability, takes over and tracks the dip latitude profile. Note that the fourth component contributes in the region east of 330°E to the west of 30°E where the impact of the second component is relatively modest. These components produce an equatorial EEJ contribution, which is opposite in sign depending on whether the dip equator is in the Northern or Southern Hemisphere. These could also be a source of the seasonal variations of the EEJ. It is not really surprising that two components are required to account for the control of the latitude of the dip equator on the variability of the strength of the observed EEJ. The region in which the fourth component dominates corresponds to the region where the location of the dip equator changes rapidly with longitude from around 13°S to 12°N. This rapid variation of the dip equator position is also accompanied by an anomalous orientation of the dip equator with respect to the geomagnetic field. The two are not perpendicular to each other as required by the classical picture of the equatorial EEJ. In the zone just east of 300°E longitude, the deviation from the expected perpendicularity is around 12° [*Jadhav et al.*, 2002]. We would expect that the response of the EEJ to changes in tidal forcing should be

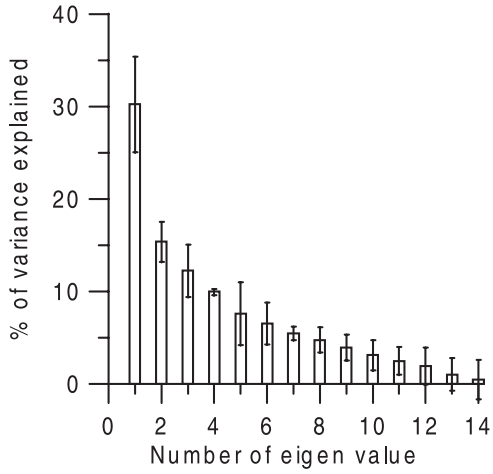

Figure 11. Percentage of variance accounted for by the first four components.

different in such a zone and it is therefore not surprising that an additional component manifests itself in this region.

[45] Finally, component 3, which contributes around 12.5% to the EEJ variability, is most conspicuous in the regions where the dip and geographic latitudes coincide. It is this component that contributes to the anomalously early peak in the 200°E region.

[46] It should be pointed out that the first four components together account for a little over two thirds of the variability of the EEJ. The other components that are responsible for the remaining contribution to the variability in EEJ could be because of various other processes including the presence of nonmigrating tides. While we have chosen only geomagnetically quiet days for our study, it is still possible that some contribution may come from the disturbance dynamo effects associated with the electric fields propagated from the auroral zone. The errors inherent in the determination of the EEJ parameters could also be responsible for the apparent variability not explained by the first four components. We have concentrated on the longitudinal structure of EEJ component. No attempt has been made to determine $D_k(d_i)$, the contribution of the kth component of day d_i, which requires EEJ contribution on a given day from all 18 longitudinal bins.

8. Results and Discussion

[47] Using an objective method for determining the parameters of the EEJ, we have shown that magnetic field observations obtained from the Ørsted satellite can form an excellent database for studying not only the longitudinal structure of the equatorial EEJ but also the sources responsible for its variations from day to day. The consistency in the correlation of the ground observations and the corresponding field computed from the deduced satellite parameters, for both the Indian and American sectors and reproduction of salient features obtained earlier [*Onwumechili*, 1997] using Pogo data, is very encouraging. It should, however, be cautioned that no claim is made that the identification of the parameters is accurate on a pass-to-pass basis. There is, however, compelling evidence to show that the deduced parameters can reproduce statistically consistent characteristics of the EEJ. Many of these features cannot be explained on the basis of the conductivity distribution in the equatorial ionosphere and longitude-dependent (migratory) tidal forcing has to be necessarily invoked.

[48] By far the most far-reaching results obtained through the analysis presented here are the conclusions based on the correlation analysis of the variability of the EEJ strength in different longitude sectors. When the correlation matrices are subjected to the principal component analysis a very clear picture emerges. Almost two thirds of the variability in the global variation of EEJ can be accounted for by the first four components taken together. The individual components describe the global as well as longitude dependence of day-to-day variability. Most significantly the importance of the geographic latitude of the dip equator in the response of the EEJ to the day-to-day changes in the global forcing is most effectively brought out by the analysis. These results are fairly robust and reveal many interesting features hitherto unnoticed. The technique appears to be very promising and could find more critical application as more of the data from the Ørsted satellite gets analyzed.

[49] It is quite remarkable that the position of the EEJ axis deduced from satellite exhibits a local time dependence similar to what has been observed on ground [*Fambitakoye and Mayaud*, 1976] being closest to the dip equator around noon. There is also a clear indication that the EEJ strength weakens as the axis moves away from the dip equator. These features appear in the global average, but the data set used is not large enough to make a statistically reliable study of the longitudinal structure of this phenomenon.

[50] The distribution of the EEJ currents in longitude is season and LT dependent and the two controlling factors cannot be separated given the limited amount of data available and the season-dependent LT of the satellite passes. The Ørsted is continuously providing data and promises to provide the source for a more complete statistics, and this deficiency will be overcome. The vector data may also provide vital information especially with regard to the importance of meridional currents.

[51] **Acknowledgments.** We are grateful for support of the Ørsted Project Office and the Ørsted Science Centre at the Danish Meteorological Institute. The Ørsted Project is funded by the Danish Ministry of Transport, Ministry of Research and Information Technology and Ministry of Trade and Industry. Additional support was provided by National Aeronautics and Space Administration (NASA), European Space agency (ESA), Centre Nationale d'Etudes Spatiales (CNES) and Deutsche Agentur fur Raumfahrtangelegenheiten (DARA). We are very thankful to WDC-C2, Kyoto, for making available the Dst indices and magnetic field data at Huancayo for downloading from their site on the Internet. We are also grateful to Dr. G. K. Rangarajan for guiding us in the acquisition of magnetic data at Fuquene and Jose William Arias for providing Fuquene observatory magnetic data.

[52] Janet G. Luhmann thanks Joseph Cain and R. G. Rastogi for their assistance in evaluating this paper.

References

Behannon, K. W., and N. F. Ness, The design of numerical filters for geomagnetic data analysis, *NASA Tech. Note, D-3341*, 1966.

Bhargava, B. N., and A. Yacob, The electrojet field from Satellite and surface observations in the Indian equatorial region, *J. Atmos. Terr. Phys.*, *35*, 1253–1255, 1973.

Cain, J. C., and R. E. Sweeney, The Pogo data, *J. Atmos. Terr. Phys.*, *35*, 1231–1247, 1973.

Chandra, H., H. S. S. Sinha, and R. G. Rastogi, Equatorial electrojet studies from rocket and ground measurements, *Earth Planet. Space*, *52*, 111–120, 2000.

Ducruix, J., V. Courtlillot, and J. L. LeMouel, Induction effects associated with the equatorial electrojet, *J. Geophys. Res.*, *82*, 335, 1977.

Fambitakoye, O., and P. N. Mayaud, Equatorial electrojet and regular daily variation SR, II, The centre of the equatorial electrojet, *J. Atmos. Terr. Phys.*, *38*, 19–26, 1976.

Gnanadesikan, R., *Methods for Statistical Data Analysis of Multivariate Observations*, John Wiley, New York, 1977.

Jadhav, G. V., M. Rajaram, and R. Rajaram, Main field control of the equatorial electrojet: A preliminary study from the Ørsted data, *J Geodyn.*, *33*(1–2), 157–171, 2002.

James, M. E., D. Tripathi, and R. G. Rastogi, Day-to-day variability of ionospheric current system, *Indian J. Radio Space Phys.*, *25*, 36–43, 1996.

Langel, R. A., M. Purucker, and M. Rajaram, The equatorial electrojet and associated currents as seen in Magsat data, *J. Atmos. Terr. Phys.*, *55*(9), 1233–1269, 1993.

Maeda, H., T. Iymori, T. Araki, and T. Kamei, New evidence of a meridional current system in the equatorial ionosphere, *Geophys. Res. Lett.*, *9*, 243–245, 1982.

Neubert, T., et al., Ørsted satellite captures high-precision geomagnetic field data, *Eos Trans. AGU*, *82*(7), 81, 87, 88, 2001.

Oko, S. O., C. A. Onwumechili, and P. O. Ezema, Geomagnetically quiet day ionospheric currents over the Indian sector, II, Equatorial electrojet currents, *J. Atmos. Terr. Phys.*, *58*(5), 555–564, 1996.

Olsen, N., et al., Ørsted initial field model, *Geophys. Res. Lett.*, *27*, 3607–3610, 2000.

Onwumechili, C. A., and C. E. Agu, Longitudinal variation of equatorial electrojet parameters derived from Pogo satellite observations, *Planet Space Sci.*, *29*, 627–634, 1981.

Onwumechili, C. A., *The Equatorial Electrojet*, Gordon and Breach, New York, 1997.

Rajaram, M., and R. Rajaram, Wind & temperature structure of the equatorial middle atmosphere, *Indian J. Radio Space Phys.*, *12*, 160–168, 1983.

Rangarajan, G. K., Application of the linear prediction filters in equatorial electrojet studies, *Proc. Indian Acad. Sci., Earth Planet. Sci.*, *101*, 329–338, 1992.

Rastogi, R. G., The equatorial electrojet: Magnetic and ionospheric effects', in *Geomagnetism*, edited by J. A. Jacobs, vol. 3, chap. 7, pp. 461–525, Academic, San Diego, Calif., 1989.

Sampath, S., and T. S. G. Sastry, Results from in situ measurements of ionospheric currents in the equatorial region, *J. Geomagn. Geoelectr.*, *31*, 373–379, 1979.

Schlapp, D. M., Worldwide morphology of day to day variability of Sq, *J. Atmos. Terr. Phys.*, *30*, 573–577, 1968.

von Storch, H., Spatial patterns: EOF and CCA, in *Analysis of Climatic Variability*, edited by H. von Storch and A. Navarra, pp. 231–263, Springer-Verlag, New York, 1999.

Yacob, A., Internal induction by the equatorial electrojet in India examined with surface and satellite geomagnetic observations, *J. Atmos. Terr. Phys.*, *39*, 601–606, 1977.

G. Jadhav, M. Rajaram, and R. Rajaram, Indian Institute of Geomagnetism, N.A.F. Moos Marg, Colaba, Mumbai-400 005, India. (geeta@iig.iigm.res.in; mita@iig.iigm.res.in; rrajaram@iig.iigm.res.in)